Supplementary Document: Analytical Study of Coupling Effects for Vibrations of Cable-Harnessed Beam Structures.

Karthik Yerrapragada
PhD Candidate
Department of Mechanical and Mechatronics Engineering
University of Waterloo
Waterloo, Ontario, CANADA, N2L 3G1
email: kyerrapr@uwaterloo.ca

Armaghan Salehian*
Associate Professor
Department of Mechanical and Mechatronics Engineering
University of Waterloo
Waterloo, Ontario, CANADA, N2L 3G1
email: salehian@uwaterloo.ca

Supplementary information to the paper titled "Analytical Study of Coupling Effects for Vibrations of Cable-Harnessed Beam Structures" by Karthik Yerrapragada and Armaghan Salehian is provided in this document. Where applicable in the research paper, the readers are pointed to this document to obtain more information.

S1. Supplementary to Mathematical Modeling

In the section 2, mathematical modeling of the paper, Equations. (13a)- (13f) and (17a) - (17d) are coupled through stiffness terms. All the coordinates of motion are coupled because of the pre-tension in the cable, Young's modulus and radius of the cable. In mathematical terms, the first derivative of displacement represents the slope, second derivative represents moment, third derivative represents shear and the fourth derivative represents the intensity of load. Mathematically, Equations. (17b) and (17c) corresponding to the in-plane and out-of-plane bending coordinates. The axial and torsion coordinates are coupled to these modes because of equivalent shear terms (third derivative of displacement and second derivative of angle). The torsion mode Equation. (17d) is coupled to the in-plane and out-of-bending modes because of equivalent moment terms. The axial mode Equation. (17a) is coupled to the bending coordinates because of equivalent shear terms. Equations (17b) and (17c) show that the coupling term related to the in-plane and out of plane bending is fourth derivative which physically corresponds to load. In Timoshenko model, Equations (13a)-(13f), the coupling coefficients in addition to depending on the cable parameters like position coordinates along y and z axis, cable radius and cable pre tension, also depends on the geometry of the host structure. In a Timoshenko beam, apart from the cable coupling, the rotation of cross section are geometrically coupled to the bending coordinates. In Equation (13a), the axial mode is coupled to the rotations of cross-sections through the cable parameters. In Equation (13b), the in-plane bending mode is coupled to the torsion mode through the cable parameters and to the rotation of cross-section about z axis because of geometry of the beam (c_{11}). Similarly, in Equation (13c) the out of plane bending mode is coupled to the

torsion mode through cable parameters and to the rotation of cross-section through the geometric term. In Equation (13d), the torsion mode is coupled to the bending terms through the cable parameters. Similarly, in Equations (13e) and (13f), the rotations of cross-section about z and y-axis are coupled to other coordinates through the cable parameters and beam geometry terms. In Timoshenko beam, we can also observe that unlike Euler-Bernoulli, we do not see presence of in-plane bending terms v in the out of plane bending mode equation w (Equation (13c)) and vice-versa (Equation (13b)). The two bending terms here are coupled through the rotations of cross-section related terms (Equations (13e) and (13f)).
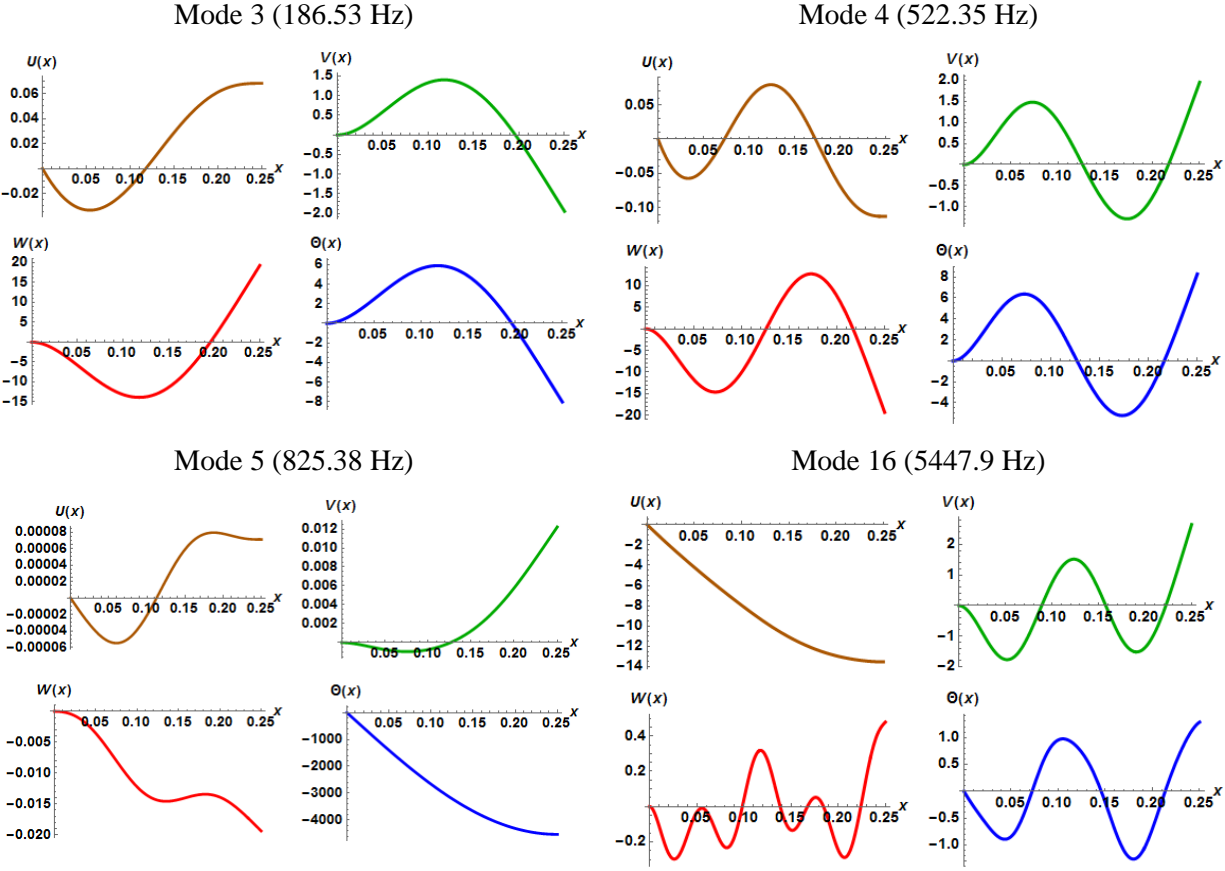
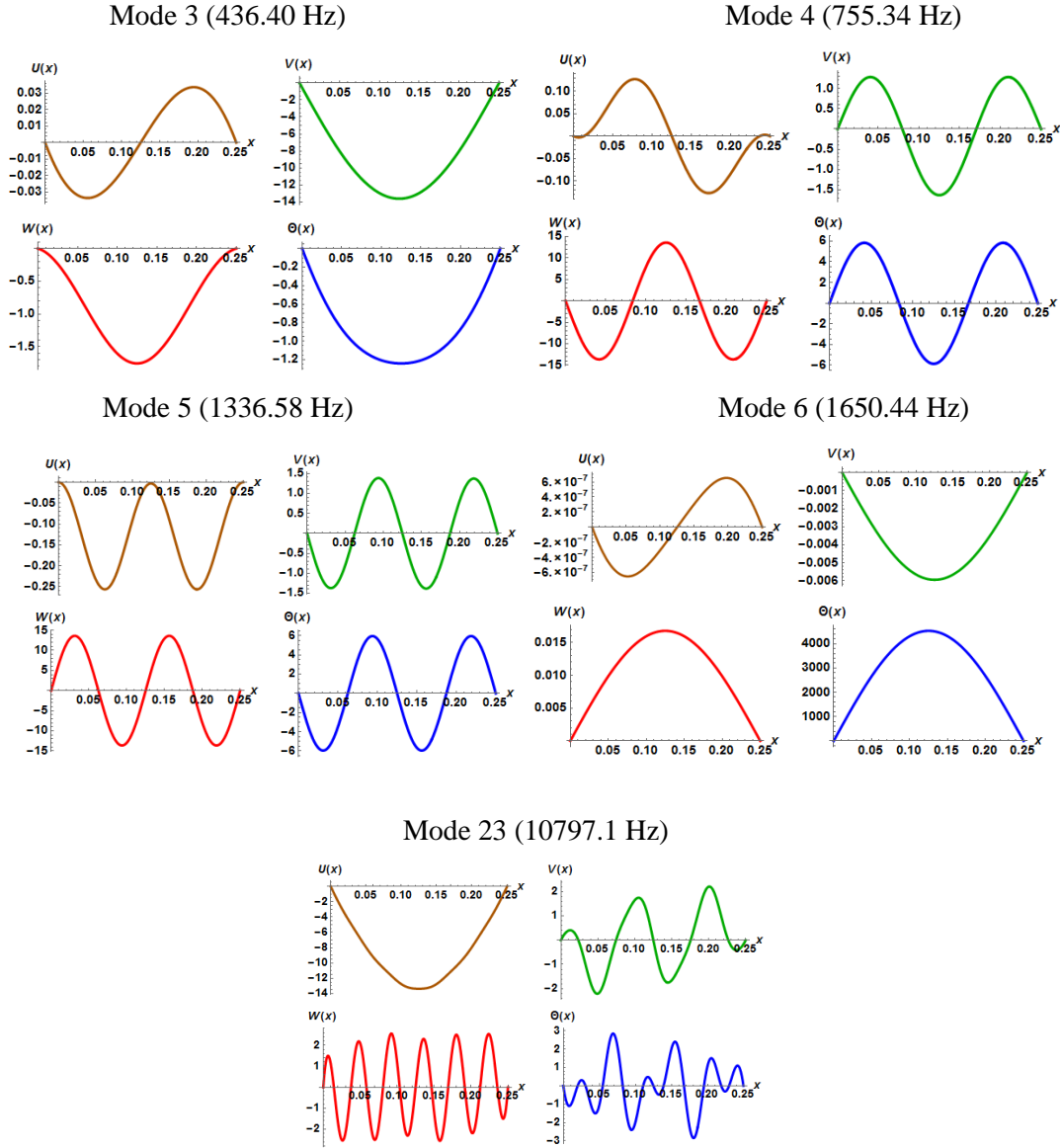## S2.   Supplementary to Results and Discussions section.

a)
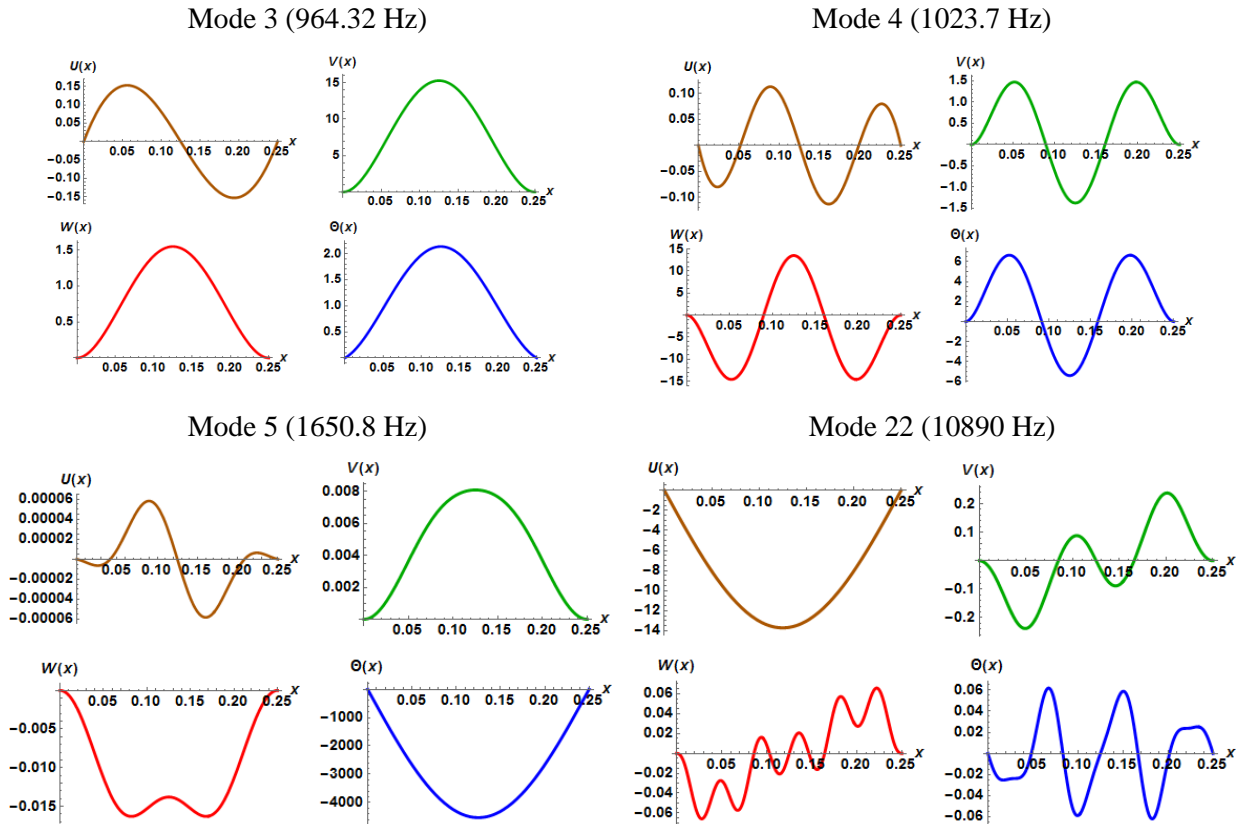
Fig s1: Vibrations mode shapes for fixed-fixed boundary conditions using coupled EB theory for Out of plane bending dominant (Mode 4), In plane bending dominant (Mode 3), Torsion dominant (Mode 5) and Axial dominant (Mode 22).

For the mode shape analysis, the mass normalized mode shapes obtained from the coupled Euler Bernoulli model are presented. The results in Figure. (s1) for fixed-fixed boundary condition indicate that for the 4th mode, the out-of-plane bending is the dominant mode. The 3rd mode is predominantly an in-plane bending mode, and the 5th mode is the torsional mode. The first predominantly axial mode is also shown in this figure, which corresponds to the 22nd mode.

Fig s2: Vibrations mode shapes for cantilever boundary conditions using coupled EB theory for Out of plane bending dominant (Modes 3 and 4), Torsion dominant (Mode 5) and Axial dominant (Mode 16).

Mode 3 (436.40 Hz)

Mode 4 (755.34 Hz)

Mode 5 (1336.58 Hz)


Mode 6 (1650.44 Hz)

Mode 23 (10797.1 Hz)

Fig s3: Vibrations mode shapes for simply supported boundary conditions using coupled EB theory for Out of plane bending dominant (Modes 4 and 5), In plane bending dominant (Mode 3), Torsion dominant (Mode 6) and Axial dominant (Mode 23).

The mode shape results in Figure. (s2) pertain to the cantilever boundary conditions. For this boundary condition, it is shown that the out-of-plane bending is dominant in the third and the fourth modes; the torsional mode is dominant at the fifth frequency, and the sixteenth mode shown corresponds to the first axial mode. For the simply supported boundary condition, Figure. (s3), the out-of-plane bending is dominant in the first, second, fourth and the fifth modes. In-plane bending is dominant in the third mode. Torsion is dominant in the sixth mode, and the mode 23 shown relates to the axial dominant mode. In the modes 5, 22 of Figure. (s1), modes 5, 16 of Figure (s2) and modes 5, 23 of Figure. (s3) respectively, due to

the effect of coupling, coordinates of motion related to the in-plane bending, out-of-plane bending and the torsion exhibit different behavior when compared to the decoupled theory. Mathematically speaking, the mode shape expression for each coordinate of motion includes the effect of all wave numbers $(\alpha_1 - \alpha_{12})$. For example, in mode 5 of Figure (s1), consider the out of plane bending curve, $W(x)$, mode 5 is a torsion dominant mode. So the mode shape parameters α related to torsion also contribute significantly to the out of plane bending response. As a result, we see distinct behavior in the mode shape of out of plane bending for mode 5 of Figure (s1) when compared to the decoupled model. The same explanation related to the dominance of the mode shape parameter α can be extended to other modes for all the boundary conditions wherever distinct behavior is seen.

b)

$$\omega_1 = 87.05\ Hz \qquad\qquad\qquad \omega_2 = 439.59\ Hz$$

(a)   (b)
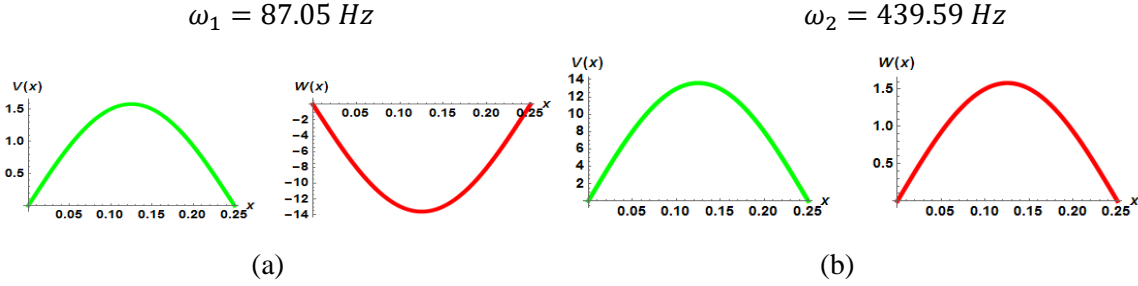
Fig s4: Mode shapes corresponding to n=1 for the system with coupled bending at $0.0043\ m$ cable offset position

After substituting the general solution in the coupled PDEs (Equations (29a) and (29b)) in the paper and converting the simultaneous algebraic equations into the matrix form, we obtain the following equation (s1).

$$\begin{bmatrix} -\dfrac{b_2 n^4 \pi^4}{l^4} + k_2 \omega^2 & -\dfrac{b_5 n^4 \pi^4}{l^4} \\[2ex] -\dfrac{b_5 n^4 \pi^4}{l^4} & -\dfrac{b_3 n^4 \pi^4}{l^4} + k_3 \omega^2 \end{bmatrix} \begin{Bmatrix} V \\ W \end{Bmatrix} = \begin{Bmatrix} 0 \\ 0 \end{Bmatrix} \tag{s1}$$

For the system to have a non-trivial solution, the determinant of the matrix in Equation. (s2) should vanish.

$$\frac{b_2 b_3 n^8 \pi^8}{l^8} - \frac{b_5^2 n^8 \pi^8}{l^8} + \left(-\frac{b_3 k_2 n^4 \pi^4}{l^4} - \frac{b_2 k_3 n^4 \pi^4}{l^4} \right) \omega^2 + k_2 k_3 \omega^4 = 0 \tag{s2}$$

Solving Equation. (s2) for ω, we obtain the expressions for the natural frequencies as follows as shown in Eq. (32) of the paper.

$$\omega_1 = \sqrt{\dfrac{\dfrac{b_3 k_2 n^4}{l^4} + \dfrac{b_2 k_3 n^4}{l^4} - \dfrac{\sqrt{(b_3 k_2)^2 n^8 - 2 b_2 b_3 k_2 k_3 n^8 + 4(b_5)^2 k_2 k_3 n^8 + (b_2 k_3)^2 n^8}}{l^4}}{2 k_2 k_3} \pi^2}$$

$$\omega_2 = \sqrt{\dfrac{\dfrac{b_3 k_2 n^4}{l^4} + \dfrac{b_2 k_3 n^4}{l^4} + \dfrac{\sqrt{(b_3 k_2)^2 n^8 - 2 b_2 b_3 k_2 k_3 n^8 + 4(b_5)^2 k_2 k_3 n^8 + (b_2 k_3)^2 n^8}}{l^4}}{2 k_2 k_3} \pi^2}$$

(s3)

The next step is to plot the mode shapes. The spatial solutions can be obtained by satisfying the linear dependency criterion for the following equation.

$$\left(-\frac{b_2 n^4 \pi^4}{l^4} + k_2 \omega^2\right) V + \left(-\frac{b_5 n^4 \pi^4}{l^4}\right) W = 0$$

(s4)

Therefore, the coupled mode shapes for $n = 1$ of the system are as follows.

$$V(x) = b_m \left(\frac{b_5 \pi^4}{l^4}\right) \sin\left(\frac{\pi x}{l}\right) \qquad\qquad W(x) = b_m \left(-\frac{b_2 \pi^4}{l^4} + k_2 \omega^2\right) \sin\left(\frac{\pi x}{l}\right)$$

(s5)

The mode shape constant b_m can be found out by using the following mass normalization criterion.

$$\int_0^l \left(k_2 V_n(x) V_n(x) + k_3 W_n(x) W_n(x)\right) dx = 1$$

(s6)

The coupled mode shapes corresponding to the lower and higher natural frequency roots of Equation. (32) are plotted in Figures. s4 (a) and s4 (b) respectively. In Figure s4 (a), the mode shapes corresponding to the out of plane bending and in-plane bending are out of phase with each other. The magnitudes for the mass normalized mode shapes shown in this figure indicates that the lower root corresponds to the out-of-plane bending dominant mode, and the other corresponds to the in-plane bending.

c)
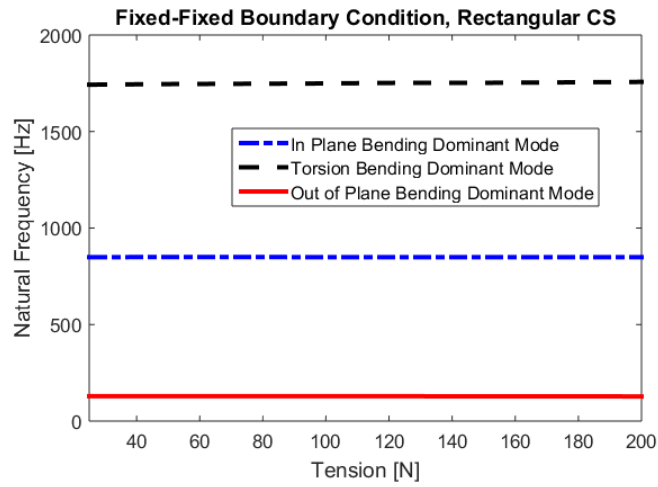
Fig s5: Effect of cable pre-tension on the natural frequencies for first in-plane bending, out-of-plane bending and torsional mode using the system parameters of Table (1) of the paper.

Figure (s5) shows the natural frequency variations for the first in-plane and out-of-plane bending and torsional modes with respect to the cable pre-tension for the system parameters shown in Table (1) of the paper. From this figure, it can be understood that the pre-tension has negligible effect on the system's natural frequencies. This is because of the relatively large bending stiffness that makes it less susceptible to the effects of tension.

d)
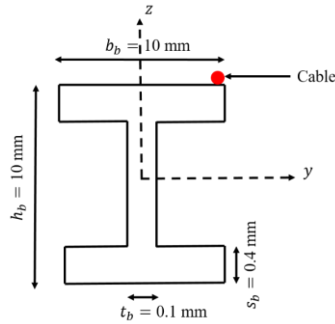
Fig. s6: I-beam cross section and dimensions

Table. s1: Material and geometrical properties for the tension case study, I-cross section beam

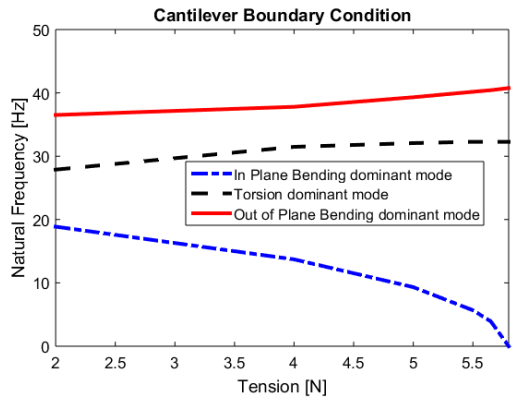| System parameters	Value
Beam length	0.25 m
Beam density	1,300 Kg/m^3
Beam modulus of elasticity	1 GPa
Beam shear modulus	0.35 GPa
Beam Poisson's ratio	0.4
Cable radius	0.0002 m
Cable density	1,200 Kg/m^3
Cable modulus of elasticity	1.1 GPa

To further, study the impact of tension on the natural frequencies, an I-beam cross-section shown in Figure. (s6) (Front View) with the numerical parameters presented in Table (s1) is also considered. The position coordinates of the center of the cable in this case are $(y_c, z_c) = (0.0048, 0.0052)\ m$. This geometry was chosen due to its smaller torsional stiffness. As shown in Figure. (s7a), the fundamental mode for the fixed-fixed boundary condition corresponds to the torsional dominant mode. In Figures. (s7b) and (s7c), for cantilever and simply supported boundary conditions, the fundamental mode corresponds to the in-plane bending dominant mode.

As expected for the I cross-section, the in-plane bending has much smaller critical loading compared to the out-of plane bending due to the smaller moment of inertia in that direction. Therefore, the in-plane bending is shown to be more prone to buckling in Figures. (s7b) and (s7c). Also, the critical loading for the simply supported is shown to be larger than the cantilever beam as expected. For fixed-fixed boundary condition, because the torsion mode is the fundamental one, the I section beam experiences torsional buckling. For cantilver and simply supported boundary conditions, the system experiences buckling in the in-plane direction.
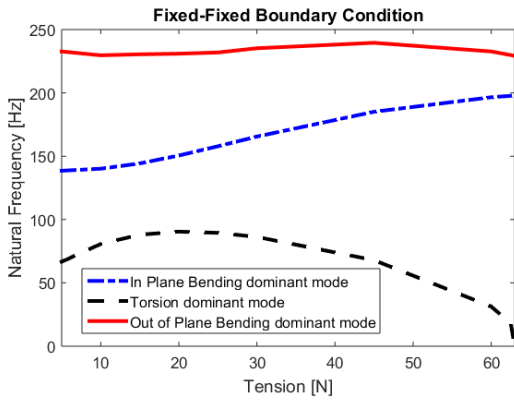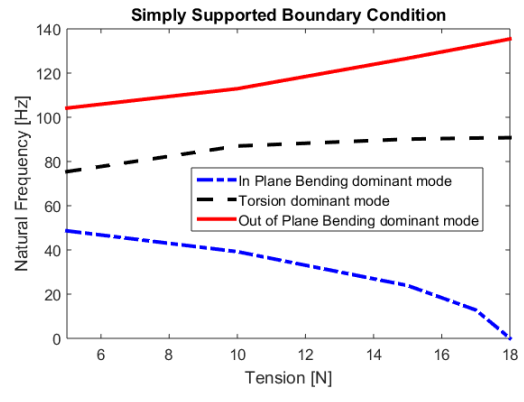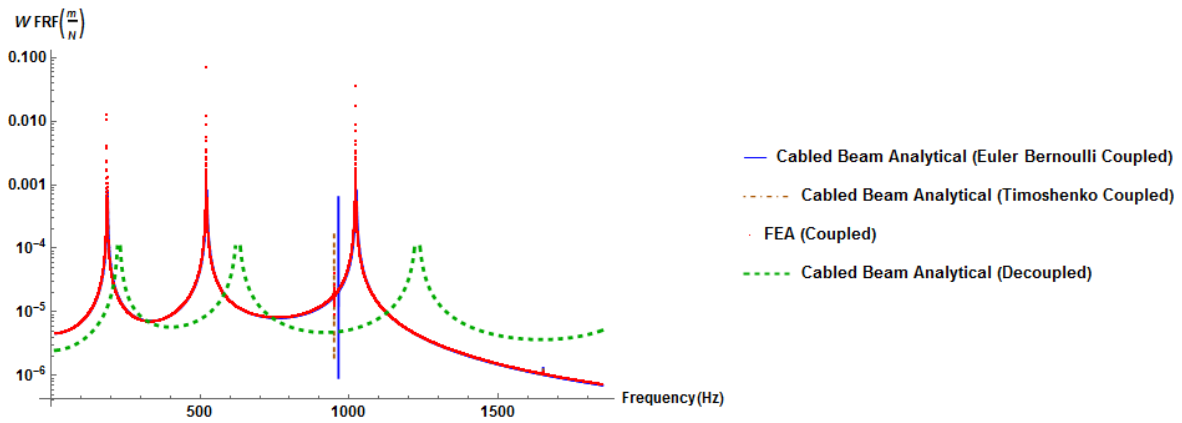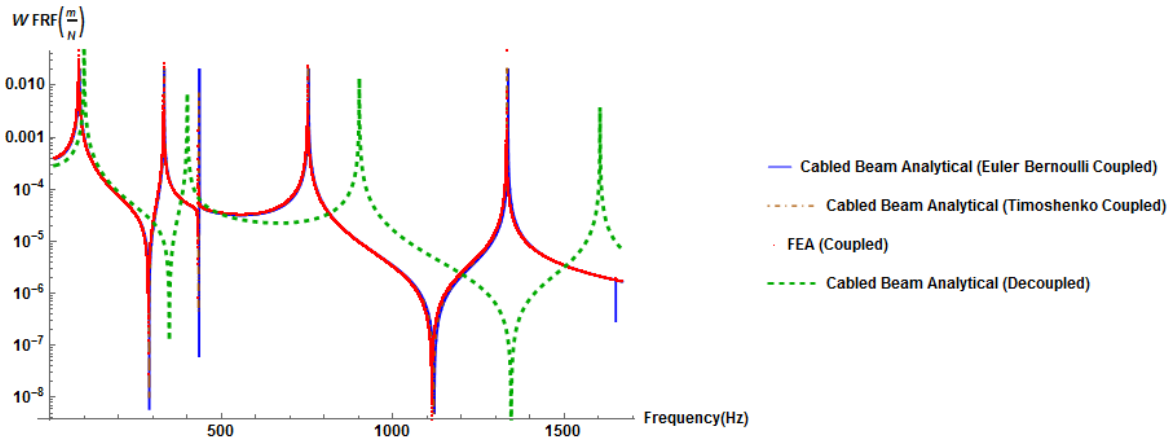
(a)

(b)

(c)

Fig s7: Effect of cable pre-tension on the natural frequencies of first in-plane bending, out-of-plane bending and torsional mode using the system parameters of Table (6) for an I-cross section beam.

e)

(a)

(b)

Fig s8: Frequency response functions for a) Fixed-fixed b) Simply Supported boundary conditions.

The sensing and actuation locations are $x_s = 0.2276\ m$ & $x_a = 0.0498\ m$, $x_s = 0.199\ m$ & $x_a = 0.136\ m$ respectively for fixed-fixed and simply supported boundary condition respectively.